Polymer 54 (2013) 5408–5418

Contents lists available at ScienceDirect

Polymer

journal homepage: www.elsevier.com/locate/polymer

In-situ SAXS study and modeling of the cavitation/crystal-shear competition in semi-crystalline polymers: Influence of temperature and microstructure in polyethylene

B. Xiong [a], O. Lame [a,*], J.M. Chenal [a], C. Rochas [b], R. Seguela [a], G. Vigier [a]

[a] Univ Lyon, INSA Lyon, MATEIS – CNRS UMR5510, Batiment Blaise Pascal, Campus Lyon-Tech La Doua, 69621 Villeurbanne, France
[b] CERMAV – CNRS, BP 53, 38041 Grenoble cedex 9, France

ARTICLE INFO

Article history:
Received 19 April 2013
Received in revised form
26 June 2013
Accepted 22 July 2013
Available online 31 July 2013

Keywords:
Polyethylene
Cavitation
Micro-macro modeling

ABSTRACT

This study focuses on the first occurrence of either cavitation or crystal shear in relation to temperature and microstructure during the tensile drawing of polyethylene. Four high density polyethylenes covering a range of crystallinity have been thermally treated to generate different microstructures displaying a large range of crystal thickness from 8 to 29 nm. The testing temperature spanned the domain 25 −100 °C. In-situ SAXS measurements on synchrotron have been performed to capture the initiation of cavitation in parallel with stress-strain measurements. Depending on microstructure and temperature the strain onset of cavitation proved to be either before or after yielding associated with homogeneous or localized cavitation regimes respectively. The transition between the two regimes can be defined by a critical value of lamella thickness at each temperature. A physical modeling based on a thermally activated nucleation process has been developed for predicting the macroscopic stress for generation of cavities as well as the one for initiating crystal shearing. This modeling accounts for both temperature and microstructure effects on yielding. It allows describing successfully the delayed apparition of cavitation with increasing temperature and decreasing crystal thickness. The observation of complete disappearance of cavitation at high temperature is also predicted by the model in relation to crystal thickness. The more relevant aspects as well as the shortcomings of the model are discussed in the conclusion.

1. Introduction

Semi-crystalline polymers constitute the larger part of commodity and specialty thermoplastics for structural applications so that it is a major issue to be able to predict their macroscopic mechanical behavior. Cavitation and crystal shear are two major processes involved in the plastic yielding [1–4]. It seems that these processes can be activated concomitantly or competitively under tensile loading depending on the materials structure and experimental conditions [5–26].

Historically, the interest for strain-induced cavitation in thermoplastic polymers was aroused by the discovery of crazing [1,2,27] that has been mainly studied at the mesoscale of craze widening, i.e. far beyond that of the lamellar structure for semi-crystalline polymers. Regarding crystal shear, this aspect of the plastic behavior of semi-crystalline polymers has been extensively investigated from a metallurgical standpoint owing to the similarity with metallic materials [4,28,29]. It is worth noticing that these processes are precursory to the fragmentation and fibrillar transformation of the crystalline lamellae beyond yielding, possibly accompanied with a melting-recrystallization [30,31].

Number of authors suspect that cavitation is an actual damaging process that should be considered into mechanical models. However, the contribution of cavitation has been almost ignored so far in the approaches for predicting the mechanical behavior of semi-crystalline polymers, and thermoplastic polymers in a general sense.

Experimental studies based on *in situ* bulk volume variations upon tensile loading have been published regarding the quantitative assessment of strain-induced cavitation [32–39], but there is still a great need of understanding of its mechanism of occurrence during plastic deformation. In this aim small-angle x-ray scattering (SAXS) proved to be a powerful tool owing to the very large electron density contrast between matter and voids [6–10,12–19,23–25].

* Corresponding author. Tel.: +33 47 243 8357; fax: +33 47 243 8528.
E-mail address: Olivier.lame@insa-lyon.fr (O. Lame).

0032-3861/$ – see front matter © 2013 Elsevier Ltd. All rights reserved.
http://dx.doi.org/10.1016/j.polymer.2013.07.055

Though being not able to detect cavities larger than a few hundred nanometers that generate scattering at very low scattering angles, SAXS enables capturing the very first events of cavitation.

Generally, cavities are assumed to be generated in the amorphous phase of semi-crystalline polymers. However, it is not clear whether cavitation initiates before or after yielding during tensile drawing. In their pioneer study dealing with high density polyethylene (PE), Butler et al. [6–9] observed that cavitation occurs at the yield point and concluded that it initiates after the onset of crystal shear. These authors suggested that crystal shear can favor cavity generation. In contrast, Pawlak and Galeski [14,15] claimed that cavitation can be initiated before the yield point. By comparing tensile and compressive experiments on high density PE, and polypropylene as well, the latter authors suggested that cavitation is liable to promote elementary crystal shear events.

Notwithstanding, the occurrence of cavitation under tensile drawing has been reported to strongly depend on material characteristics such as molecular weight [16,34], thermal history [14,15,18,23] and lamella orientation [10,23], as well as experimental factors such as draw temperature and strain rate [9,17,25,37]. Cavitation can eventually disappear for low crystallinity materials or for draw temperatures close to the melting point [9,17,39].

In a recent paper, Humbert et al. [23] reported and exhaustive *in situ* SAXS study of the tensile drawing of several PE materials having different molecular architectures. The materials were submitted to various crystallization treatments in order to modify the crystalline microstructure, namely the average crystal thickness and the chain topology. Chain topology enfolds interphase, tie chains and chain entanglements that directly transmit the load between crystal and amorphous phase. These mechanically active molecular items are gathered under the generic labeling of *stress transmitter* (ST). It was shown that the modifications of the materials morphogenesis greatly influenced the occurrence of cavitation. The SAXS patterns have been analyzed in the q-range relevant to the very first events of cavitation, namely its initiation. A semi-quantitative physical approach has been developed for describing the cavitation/crystal-shear competition.

The aim of the present work was to get deeper insight on the influence of temperature on the occurrence of cavitation in semi-crystalline polymers and the shearing/cavitation competition upon tensile drawing, and the incidence of the crystal thickness as well. In situ SAXS experiments were performed at various draw temperatures on the same polyethylene samples as the ones of the previous study [23] in order to extend our data library. A second major objective of the study was to develop a physical model of cavitation that could account for both microstructure and temperature. Our purpose was to base the modeling on an extension of the classical theory of nucleation.

2. Experimental

2.1. Materials

The four polymers under investigation are ethylene-hexene random copolymers provided by Total Petrochemicals. Table 1 discloses some characteristics of the four materials. The crystallization onset, T_c^{onset}, was determined by cooling from the quiescent melt at 170 °C.

2.2. Sample preparation

The polymer pellets were compression-molded into 500 μm thick sheets at 170 °C and quenched into water at room temperature (RT). The cooling rate was about 30 °C/s. These samples were labeled "quenched". Two thermal treatments were performed in order to generate two additional crystalline microstructures for every one of the four polymers. The samples hereafter designated as "annealed" were prepared by heat-treatment of quenched sheets for 15 h in a thermostatic oil bath at a temperature close to the crystallization onset T_c^{onset} (see Temperature of Heat Treatment (T_{ht}) in Table 1). The samples called "isotherm" were re-melted at 170 °C and plunged for 15 h into the same thermostatic oil bath at T_{ht}. During the two thermal treatments, the samples were kept into aluminum plates tightly jointed with a silicone rubber gasket to prevent oil contamination from the thermostatic bath.

Table 1
Initial characteristics of the polyethylenes: co-unit concentration, C_6; number-average- and weight-average molecular weights, M_n and M_w; DSC crystallization temperature onset, T_c^{onset}.

Materials	C_6 (mol %)	M_n (kDa)	M_w (kDa)	T_{ht} (°C)
PE-A	1.8	14.3	49	114
PE-B	0.8	15.8	54	113
PE-C	0.1	15.4	65	124
PE-D	0.2	15	69	123

2.3. DSC analysis

The thermal behavior of the polymers has been analyzed with a DSC7 apparatus from Perkin–Elmer at a heating rate of 10 °C/min. The temperature and heat flow scale were calibrated using high purity Indium at the same heating rate. The weight fraction crystallinity, X_c, was computed using the melting enthalpy of perfectly crystalline polyethylene $\Delta H_f^\circ = 290$ J/g [40]. The crystallization onset, T_c^{onset}, was determined according the procedure described in the Perkin–Elmer manual at a cooling rate of 10 °C/min.

2.4. SAXS characterization

Small-angle X-ray scattering experiments were carried out on the BM02 beamline of the European Synchrotron Radiation Facility (ESRF, Grenoble, France). The 2D-patterns were recorded using a CCD camera from Roper Scientific located at a distance of about 140 cm from the sample. The measurement were performed using a wavelength of 0.154 nm giving access to the range of scattering vector $0.05 < q < 0.95$ nm^{-1} that was calibrated by means of silver behenate. The data corrections including dark current, flat field response and tapper distortions were carried out using the software available on the beamline [41]. Background scattering was recorded during the same time as for experiments without sample, for every new experimental condition. Subtraction was not necessary as the background was insignificant compared with the sample scattering.

In-situ SAXS measurements were performed during tensile tests using a homemade stretching stage equipped with a 5 kN load cell and a heating chamber. The dumbbell samples having 6.5 mm in gauge length and 4 mm in width were stretched at an initial strain rate of 6.4×10^{-4} s^{-1}. The symmetric displacement of the two clamps allowed probing the same zone of the sample during the tests. In addition we have checked that the necking zone size is of the order of magnitude of the gauge length so that the nominal strain is a reasonably good indicator of the local strain of the probed zone even after necking. The pattern recording time of 5 s was chosen in order to have the best compromise between pattern resolution and minimum strain increment during the recording. The stress-strain curves were used to determine the elastic modulus of every sample using two independent recordings at each temperature. The modulus was computed from the tangent at the

origin of a 2nd order polynomial fitting on the 0–3% strain range of the experimental curves.

The long period, L_p, of the lamella periodic stacking was calculated from the correlation maximum of the Lorentz-corrected intensity profile, $I(q)q$ [2], using the Bragg's relation

$$L_p = 2\pi/q_{peak} \quad (1)$$

where q_{peak} corresponds to the apex of the correlation peak.

The crystalline lamella thickness was deduced from the following relation

$$L_c = L_p \frac{\rho}{\rho_c} X_c \quad (2)$$

where $\rho_c = 1.003$ g cm^{-3} is the density of the PE crystal and ρ is the density of the sample. This relation assumes very large extend of the crystalline lamellae with regard to thickness, as evidenced by direct AFM observations [42]. The L_p and L_c data are reported in Table 2.

The volume fraction of voids was estimated using the method already described by Humbert et al. [23] after azimuthal integration of the 2D-patterns and correction for sample thickness. The scattering intensity from voids in isotropic systems can be calculated with the following relation

$$2\pi^2(\Delta\rho)^2 V(1-V) \approx 2\pi^2\rho^2 V K_1 = \int_0^\infty I(q)q^2 dq \quad (3)$$

where V is the volume fraction of cavities. For anisotropic systems with axial symmetry, the scattering intensity should be integrated according to the following relation as given in Ref. [43]

$$2\pi^2\rho^2 V K_1 = \int_0^\infty q \int_0^{\pi/2} q\cos(\xi) I(q) dq d\xi \quad (4)$$

where ξ is the azimuthal angle. The experimental K_1 factor is a kind of calibration parameter that was determined from the scattering of the semi-crystalline material in the undeformed state according to a previously described procedure [23]. This factor should be nearly constant during drawing before the occurrence of cavitation since sample thickness changes very little as well as crystallinity. Beyond the strain onset of cavitation, K_1 should change due to modifications of thickness and transmission coefficient of the sample. However, such modifications were not taken into consideration in the present work since our goal was not to assess an absolute value of the scattering intensity but to detect and record the strain onset of cavitation for further modeling.

Table 2
Physical characteristics of the heat-treated polyethylenes.

Materials		X_c (%)	L_p (nm)	L_c (nm)
PE-A	Quenched	49	17	8
	Annealed	52	23	11
	Isotherm	53	24	12
PE-B	Quenched	54	19	9
	Annealed	62	22	13
	Isotherm	65	26	16
PE-C	Quenched	65	20	12
	Annealed	73	30	21
	Isotherm	75	36	26
PE-D	Quenched	69	22	14
	Annealed	77	30	22
	Isotherm	80	37	29

The procedure for computing the cavity volume fraction could be only performed in a limited q-window from $q_{min} \approx 0.05$ nm^{-1} as determined by the beamstop to $q_{max} \approx 0.20$ nm^{-1} corresponding to the onset of scattering by the crystalline lamella stacks. Hence, the size of the voids captured by SAXS lies in the range 30–100 nm. This means that only a small part of the voids can by analyzed by this method, the ones bigger than 100 nm being excluded from the analysis. Integration of Eq. (4) in the range $0 < q < q_{min}$ was made via a linear extrapolation ignoring the un-accessible bigger cavities. In the range $q_{max} < q < \infty$, integration was made by assuming Porod's behavior.

As pointed out by Humbert et al. [23], the smallest observable cavities are about 40 nm according to the form factor of the scattering cavities at the onset of appearance of the strong scattering from cavitation. It was thus concluded that the incipient voids quickly expand to a stable size of 40 nm, the recording device being unable to capture the very moment of nucleation. The aim of the procedure is thereby not to assess the whole amount of cavities but to follow up the cavitation nucleation by an *in situ* determination of the volume fraction of the voids during their growth in the size window 40–100 nm. This procedure stands for the counting of cavity nucleation events.

3. Results and discussion

3.1. Tensile behavior and SAXS observations

Fig. 1 shows the nominal stress–strain curves of PE-C annealed as a function of the draw temperature, T_d. Both the modulus and yield stress significantly decrease with increasing T_d. This sample exhibits an inhomogeneous deformation with a neck propagation whatever T_d between RT and 100 °C. In contrast, the unreported data regarding PE-A reveal a homogeneous deformation behavior at $75 \leq T_d \leq 100$ °C without distinct yield point, whatever the thermal treatment.

SAXS patterns have been routinely recorded during drawing for all samples at the various draw temperatures. Only the patterns for the PE-C annealed sample are shown in Fig. 2 as an example. SAXS patterns at RT can be found elsewhere [23].

At the onset of cavitation, the scattering intensity arising from the voids is not isotropic, the central spot being significantly elongated in the tensile direction. Considering the cylindrical symmetry of the system about the draw axis, this means that the

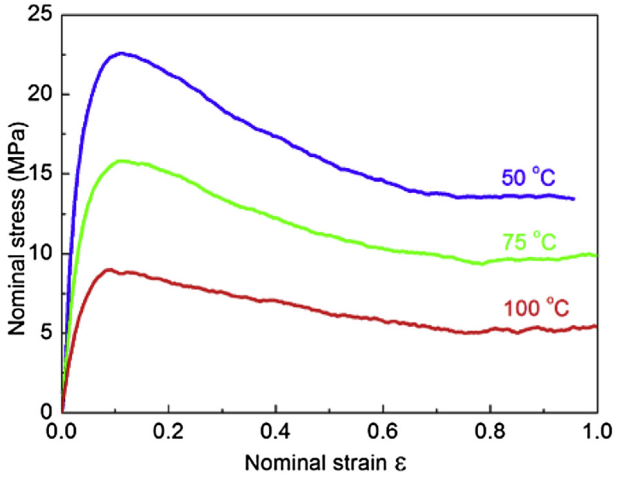

Fig. 1. Nominal stress–strain curves of PE-C annealed as a function of the draw temperature (strain rate = 6.4×10^{-4} s^{-1}).

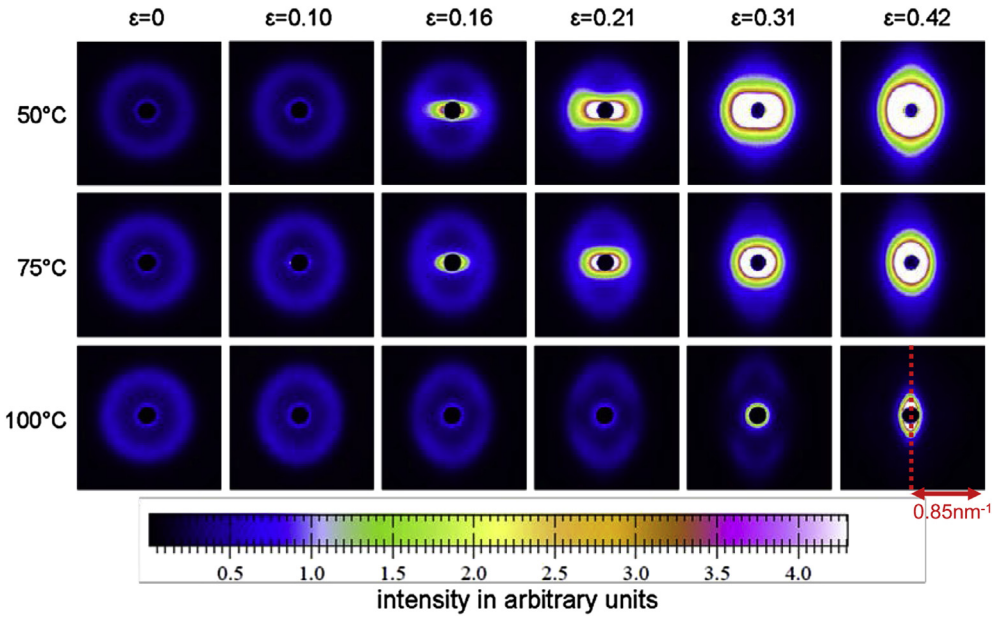

Fig. 2. SAXS patterns as a function of nominal strain for PE-C annealed at different draw temperatures (the draw axis is horizontal).

cavities have a shape of oblate ellipsoids with their major axis oriented normal to the tensile direction. With increasing strain, the cavity scattering gradually evolves into an elliptic shape transverse to the tensile direction indicating that the cavity shape changes into prolate ellipsoids elongated in the tensile direction.

Regarding the effect of draw temperature, Fig. 2 shows that the cavitation scattering from PE-C annealed is delayed at higher strains when T_d increases. This reduced trend for cavitation with increasing temperature is true for all the PE samples of the present study.

3.2. Determination of nucleation and growth of voids

Quantitative analysis of the 2D-patterns in the q-range of cavity scattering has been performed for all four samples and for the three thermal treatments. In the 2D-patterns of undeformed samples, a very slight scattering can be observed around the beamstop (Fig. 2). This scattering can be due to various kinds of unidentified structural defects that have no influence on our analysis of the data.

Fig. 3 reports several sets of data of void volume fraction computed according to the previously described method. The extremely low V values give evidence that the procedure only concerns a very low fraction of the voids as indicated in the experimental part, namely the voids which size is in the range 40–100 nm. Besides, it is to be mentioned that the SAXS recordings of strongly cavitating samples should be stopped at rather small strains due to detector saturation. This is an experimental evidence of SAXS tremendous sensitivity to small cavities.

In Fig. 3a are plotted the data regarding the drawing at $T_d = 50\ ^\circ C$ of the four PE samples submitted to the various thermal treatment. At small strain the volume fraction, V, stays constant to the initial level. This means that no strain-induced cavitation is generated in the pre-yield strain domain. For strains $\varepsilon > 5\%$, void volume fraction slowly starts to increase in parallel with deformation for samples PE-D and PE-C isotherm and annealed. Then V jumps at $\varepsilon \approx 10\%$ for these four samples indicating a sudden and profuse occurrence of void nucleation events. In contrast, PE-B and PE-A display very little is any cavitation at $T_d = 50\ ^\circ C$. Obviously, at a given draw temperature, the cavitation propensity is directly

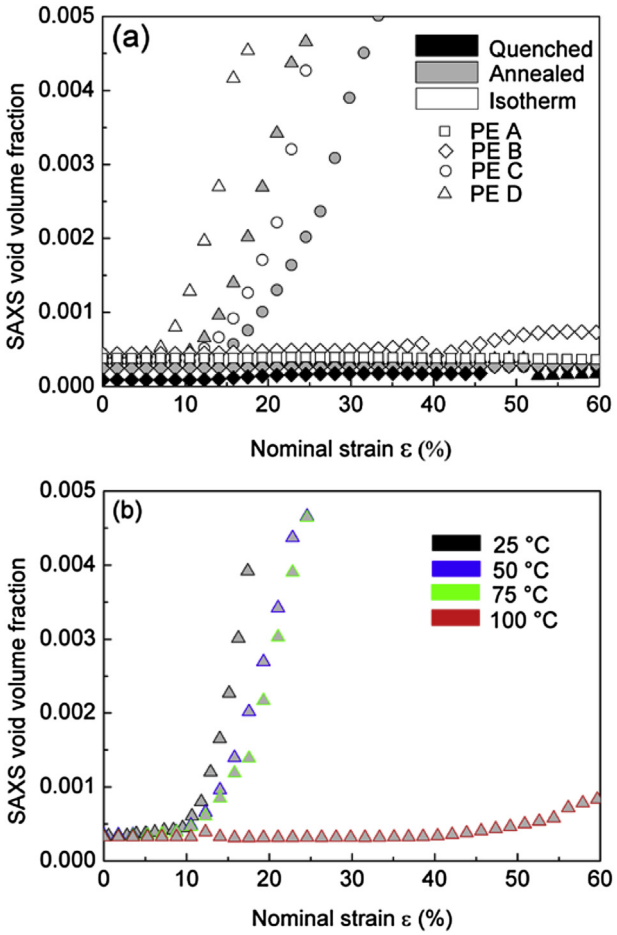

Fig. 3. Evolution of SAXS void volume fraction as a function of nominal strain (a) for the various materials at $T_d = 50\ ^\circ C$ and (b) for PE-D annealed at several draw temperatures.

connected with structural factors such as crystallinity or crystal thickness (see Table 2). Besides, the transition from the early cavitating materials to the ones exhibiting delayed cavitation is rather clear cut. This suggests that the occurrence of cavitation is ruled out by a physical criterion with regard to plastic yielding.

In Fig. 3b, the data regarding the drawing of PE-D annealed at various draw temperatures show that cavitation nucleation occurs suddenly at strain $\varepsilon \approx 10\%$ and jumps quickly with increasing strain for $T_d \leq 75\ ^\circ C$. For $T_d = 100\ ^\circ C$, no more cavitation occurs before the strain reaches $\varepsilon \approx 45\%$ which is far beyond the yield point. These latter data show that the criterion of occurrence of cavitation is highly sensitive to temperature.

The strain onset of cavitation, ε_{onset}, can be estimated from the sudden increase of void volume fraction versus strain curves as can be seen in Fig. 3a and b. Sample which do not display an increase of void volume fraction are considered as been not cavitating though some of them may display an anisotropic central scattering (see for example SAXS pattern in Fig. 2: $T_d = 100\ ^\circ C$ $\varepsilon = 0.42$). It should also be mentioned that ε_{onset} is accurately determined when cavitation occurs prior to yielding since at this stage the deformation is homogeneous so that the nominal strain is relevant. However, when located beyond the yield point, ε_{onset} is just a strain indicator since the occurrence of necking makes the deformation highly heterogeneous so that the nominal strain is irrelevant. This is not a major problem since in the following we will focus on the case of homogeneous cavitation, i.e. when an actual competition exists between cavitation and crystal shear. Indeed, in the heterogeneous case, cavitation does not actually compete with crystal shear, it is just a companion process of the fibrillar transformation.

Under these considerations, ε_{onset} has been plotted in Fig. 4 as a function of the crystal thickness, L_c, that is a convenient parameter to account for the dependence of microstructure on both the polymer nature and thermal treatment. In the range of the high ε_{onset} values of every plot, the symbols with the label ∞ stands for samples that did not exhibit cavitation within the strain range of our experiments, i.e. $\varepsilon \leq 1.0$. All the curves exhibit the same shape regardless of temperature. The general trend is a steep increase of ε_{onset} with decreasing L_c at a given T_d. This transition from low to high ε_{onset} values is relevant to a change in the occurrence of cavitation prior to or beyond yielding. The temperature sensitivity of the phenomenon is clearly evidenced by the significant shift to lower L_c with decreasing T_d. This is a clear indication that the cavitation ability is enhanced by lowering T_d at a given L_c.

From every curve of Fig. 4, a minimum value of the crystal thickness, L_c^{min}, can be determined as the one below which cavitation does not occur at a given draw temperature. The vertical broken lines are featuring the asymptotic behavior of the ε_{onset} upswing with decreasing L_c at every draw temperature. The positioning of these lines was determined by averaging the experimental L_c value associated with $\varepsilon_{onset}^{\infty}$ (no cavitation) and the nearest L_c value resulting in a measurable ε_{onset}. For $T_d = 75\ ^\circ C$, the uncertainty is quite high due to the missing of data in the very region under consideration. Extrapolations of the broken lines to the *X*-axis give the L_c^{min} value for every draw temperature of the study. The steady increase of L_c^{min} with increasing T_d can be attributed to the different thermal activations of crystal shear and cavitation. This is believed to be the origin of the competition between the two process as already pointed out by Humbert et al. [23] and Pawlak-Galeski [14]. Both groups proposed physical criteria for cavitation based on the balance between the tensile stress required for the nucleation of a cavity and that for initiating crystal shear. This point will be analyzed in more details in the *modeling* subsection.

3.3. Homogeneous versus localized nucleation of cavitation

For samples having $L_c > L_c^{min}$, cavitation can take place either prior or after yielding, so that the phenomenon proceeds homogeneously over the whole sample or locally in the necked region, respectively. The strain onset of cavitation is plotted in Fig. 5 as a function yield strain for all materials that did exhibit cavitation. The straight line $\varepsilon_{onset} = \varepsilon_{yield}$ shows the separation between the domains relevant to homogeneous and localized cavitation. With increasing draw temperature, the number of samples exhibiting cavitation gradually decreases, and among the cavitating samples fewer and fewer exhibit homogeneous cavitation prior to yielding. At $T_d = 100\ ^\circ C$, none of the less crystalline samples PE-A and PE-B exhibit cavitation, whatever the thermal treatment.

When cavities occur first in the intercrystalline amorphous phase, the process is homogeneous over the whole sample. In this case, the crystalline microstructure is still under elastic deformation conditions just after cavity nucleation. The scenario of localized cavitation takes places when crystal shear occurs prior to cavitation, the latter process being generated in the yielding regime as a result of crystal breakage. Cavitation is called localized in this case since it is located in the necked region of the sample. A third situation may take place when stress for plastic yielding is much lower than that for cavitation so that cavitation does not occur, or at least is not reached before the strain-hardening domain after complete transformation of the microstructure. This was previously

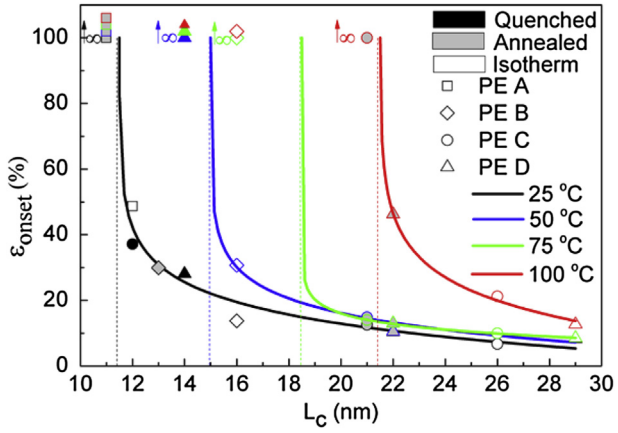

Fig. 4. Strain onset of cavitation as a function of crystal thickness and draw temperature (strain rate = $6.4 \times 10^{-4}\ s^{-1}$; estimated error on $\varepsilon_{onset} \approx \pm 3\%$).

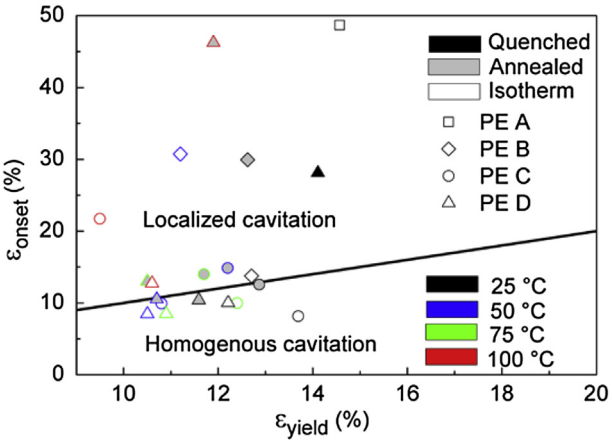

Fig. 5. Strain onset of cavitation as a function of yield strain versus draw temperature.

observed only for T_d close to the melting point for polypropylene [17] and polylactide [25]. The present data show that this also applies at RT for PE-A quenched or annealed (Fig. 4).

The evolution of the cavitation modes of the various materials as a function of the draw temperature is summarized in the sketch of Fig. 6. The ranking of the samples in the order of increasing L_c on the x-axis clearly emphasizes the prime role of this parameter on the ability for cavitation. A thoroughly opposite behavior of the materials can be observed on both sides of the diagram. On the left-hand side, cavitation never occurs at any draw temperature for quenched PE-A and PE-B, and annealed PE-A as well. In contrast, isothermally crystallized and annealed samples of both PE-C and PE-D always exhibit cavitation, either homogeneous or localized depending on T_d. In the mid range of the diagram, dual cavitation behavior is observed for the four polymers depending on their thermal treatment and T_d, i.e. either localized cavitation or no cavitation. The annealed PE-C specimen is the only one to experience all three modes from homogeneous cavitation to no cavitation with increasing T_d from 25 to 100 °C.

4. Modeling of the cavitation/crystal-shear competition

A physical approach of cavitation in semi-crystalline polymers is developed to quantitatively account for the experimental observations under uniaxial tensile drawing at various temperatures. The modeling of cavitation is based on the classical nucleation theory previously introduced by Humbert et al. [23]. The main progress consists in building up a scaling transition from the local to the macroscopic scale and taking into account the temperature effects. This approach only considers the case of homogeneous cavitation and assumes linear elasticity at every step of the modeling.

The starting point is the mechanism by which cavitation is generated and the assumption regarding the computation of the cavitation stress at a local scale in the bulk. Borrowing from Mourglia [45], a classical nucleation theory involving both surface and volume energy contributions can be used. The above author supposed that the energy relaxed when a cavity is generated includes a surface energy contribution associated with the new surface generated by the cavity and a local elastic energy contribution that can be written in the form $K\varepsilon_v^2 dV$, where K is the bulk modulus and ε_v the volume strain. This model was conceived for solid material such as glassy polymers but less relevant for liquids or rubbers. The glass transition temperature of polyethylene is far below room temperature so that the amorphous phase confined between two neighbor crystallites is rubbery for the testing conditions of the present study. As a consequence the elastic stress about an incipient cavity can relax over the whole volume of the rubber phase, so that the relaxed elastic energy should have the form $K\varepsilon_v dV$. The potential energy, φ, representative of the material state can be then expressed as

$$\varphi = -\frac{4}{3}\pi r^3 K\varepsilon_v + 4\pi r^2\gamma \tag{5}$$

where γ is the surface tension of the material, and r is the radius of the cavity. The definition of such a potential allows determining a critical radius, r_c, for a stable cavitation nucleus from the derivate $(d\varphi/dr)_{r=rc} = 0$, and a potential barrier $\Delta\varphi$ for reaching the critical value $\varphi(r_c)$. Therefore, it comes straightforwardly that

$$\Delta\varphi = \frac{16\pi\gamma^3}{3\left(K\varepsilon_v^{cav}\right)^2} = \frac{16\pi\gamma^3}{3\sigma_v^{cav^2}} \tag{6}$$

where σ_v^{cav} and ε_v^{cav} are the critical values of the volume stress (i.e. hydrostatic stress) and the volume strain for the generation of a cavity.

In the theory of thermal activation processes, the nucleation potential barrier is assumed to obey the classical temperature-dependent relation

$$\Delta\phi = \delta k_b T \tag{7}$$

where k_b is the Boltzmann constant. The δ factor only accessible from experiments is strongly dependent on experimental conditions [46]. In the present study δ should be a constant since experimental conditions are unchanged for all materials except temperature that is specifically taken into account in Eq. (7). So, σ_v^{cav} and ε_v^{cav} for cavitation in a bulk rubbery material are given by the following relations

$$\sigma_v^{cav} = \sqrt{\frac{16\pi\gamma^3}{3\delta\, k_b T}} \quad \text{or} \quad \varepsilon_v^{cav} = \sqrt{\frac{16\pi\gamma^3}{3K^2\delta\, k_b T}} \tag{8}$$

The model relies on the above equations that are used as a cavitation criterion at a local scale in the rubbery layers of semi-crystalline PE, in order to perform the scaling transition towards the macroscopic behavior. A schematic of the approach is shown in Fig. 7 that displays an intermediate step at the nanoscale of lamella stacks. This approach involves both physical considerations and experimental findings. Only the equatorial regions of the spherulites are taken into account since cavitation should preferentially initiate in the rubbery amorphous phase confined between the crystal lamellae normal to the tensile stress due to the favorable situation with negative hydrostatic stress [47].

It is first assumed at a microscopic scale that the volume strain in the amorphous layer of the semi-crystalline polymer, ε_v, is proportional to the axial strain, ε_z^a, so that

$$\varepsilon_v = B\varepsilon_z^a \tag{9}$$

where B is a coefficient mainly dependent on the material morphology. Indeed, this coefficient is physically related to the local stress state of the amorphous phase confined between the crystallites in the stacks: $B = 1$ for purely oedometric state of stress that stands for highly crystalline polymers with very high lamella shape factor, $f =$ width/thickness; $B = 0$ for isochoric biaxial state in the case of low crystallinity polymers with narrow lamella stacks and thick amorphous layers. AFM observations [42] performed on the materials of the present study revealed that the lamella shape

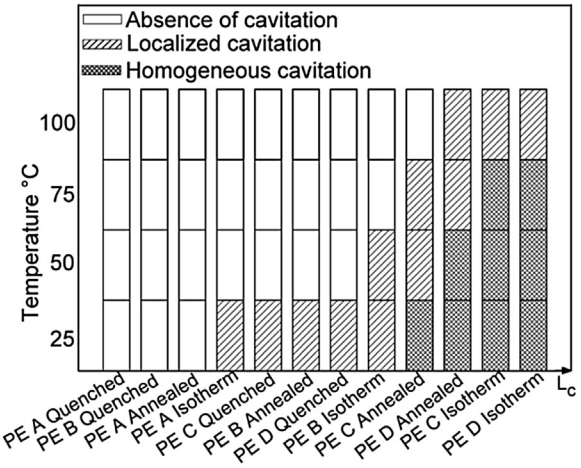

Fig. 6. Schematic evolution of the cavitation mode in relation to the crystal thickness of the various materials and the draw temperature.

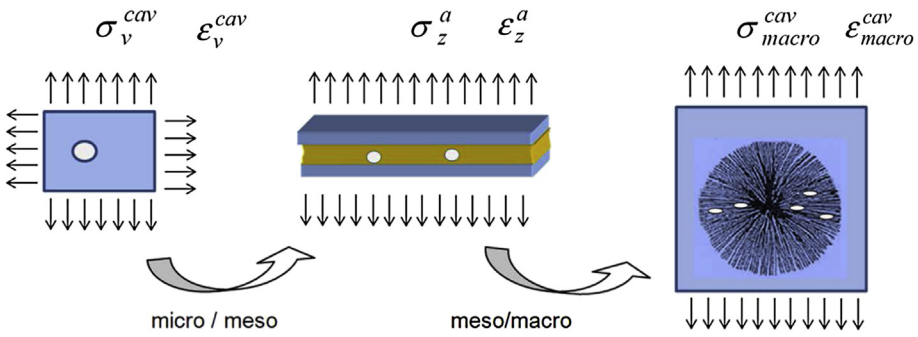

Fig. 7. Schematic pathway of the scaling transition from the micro to the macro level of structure for the calculation of the macroscopic stress of cavitation initiation.

factor spans the range $20 < f < 100$ depending on the crystallinity. Besides, it was shown on theoretical grounds [47] that in a stack of alternating soft and stiff layers under tensile testing the volume stress does not change significantly in the f range mentioned above. This means that the state of stress and strain in the soft layers is roughly insensitive to f changes in the range $20 < f < 100$. Therefore, one may reasonably assume that the B factor of Eq. (9) is fairly constant for the present materials. Moreover, considering that B is essentially structure-dependent, one should expect very little sensitivity to temperature, if any.

In parallel to Equation (9) one may also assume a linear elastic behavior at the microscopic scale of the confined amorphous layer

$$\sigma_v = K\varepsilon_v \tag{10}$$

where σ_v is the volume stress and K the bulk modulus of the amorphous phase.

A step ahead in the scaling transition can be made by considering that the crystalline layer in the lamella stacks is much stiffer than the amorphous layer, so that the microscopic strain in the amorphous layers, ε_z^a, can be related to the mesoscopic strain of the stack by

$$\varepsilon_{meso} = \varepsilon_z^a L_a / L_p \tag{11}$$

where the mesoscopic strain, ε_{meso}, comes from SAXS measurements, and $L_p = L_a + L_c$ is the long period, L_c and L_a being the thicknesses of the crystalline lamellae and the amorphous layers respectively.

The next step in the scaling transition is then to establish a relationships between the mesoscopic scale of the lamella stacks and the macroscopic scale, for both stress and strain. Experimental data from a previous SAXS study [48] showed that the mesoscopic to macroscopic strain ratio at room temperature is nearly crystallinity independent in the range $50\% < X_c < 80\%$, for the same materials as those of the present study. Besides, from the present SAXS data it turned out that this coefficient remains roughly crystallinity independent at each temperature [49]. These experimental findings afford a base for the meso-macro scaling transition which can be written as

$$C(T) = \varepsilon_{meso}/\varepsilon_{macro} \tag{12}$$

where ε_{macro} is the macroscopic strain during a tensile test. The macroscopic strain can be given a more explicit form as

$$\varepsilon_{macro} = \varepsilon_z^a \frac{L_a}{L_p}\frac{1}{C} \tag{13}$$

Assuming a linear elastic behavior of the material at the macroscopic scale

$$\varepsilon_{macro} = \sigma_{macro}/E \tag{14}$$

where E is the elastic modulus of the bulk material and σ_{macro} the macroscopic stress, combining Eqs. (13) and (14) results in

$$\sigma_{macro} = \varepsilon_z^a \frac{E}{C}\frac{L_a}{L_p} \tag{15}$$

Then using Eqs. (9) and (10), Eq. (15) turns into

$$\sigma_{macro} = \sigma_v \frac{E}{C\,K\,B}\frac{L_a}{L_p} = \sigma_v \frac{E}{C\,K\,B}(1-\phi_c) \tag{16}$$

where $\phi_c = 1 - L_a/L_p$ is the crystal volume fraction.

Finally, Equation (16) can be written for the specific case of the cavitation onset by changing σ_v for σ_v^{cav}. This gives the next relation for the macroscopic stress for cavitation

$$\sigma_{macro}^{cav} = \sigma_v^{cav}\frac{E}{C\,K\,B}(1-\Phi_c) = \sqrt{\frac{16\pi\gamma^3}{3\delta\,k_b T}}\,\frac{E}{C\,K\,B}(1-\phi_c) \tag{17}$$

This later equation accounts for the 2-step scaling transition from the single cavity nucleating in a homogeneous medium to the macroscopic behavior of the semi-crystalline material under uniaxial stress. It is a function of both temperature and microstructure. However, based on the quantitative data of the various parameters of Eq. (17) reported in Table 3, the dependence of σ_{macro}^{cav} on crystallinity is expected to be rather weak in contrast to that of σ_v^{cav}. Indeed, C, K and B are roughly independent of microstructure (X_c or L_c), whereas E is an increasing function of X_c (or L_c) [50] but this dependence should be counterbalanced by the factor $(1-\phi_c)$.

Experimental determination of σ_{macro}^{cav} can be performed from the nominal stress/strain curves at the strain onset of cavitation, ε_{onset}, as determined from SAXS. Here, ε_{onset} is considered to be equivalent to $\varepsilon_{macro}^{cav}$ (see Fig. 7). Only the cases of homogeneous cavitation have been taken into consideration. Indeed, the localized cavitation is associated with the occurrence of plastic necking prior

Table 3
Evolution trends of the physical parameters of the cavitation model as a function of temperature (25 °C < T < 100 °C) and microstructure (9 nm < L_c < 29 nm).

Parameter	T: 25 °C ↗ 100 °C				L_c: 9 nm ↗ 29 nm			
$(1-\phi_c)$	~cst				0.54	↘		0.22
E (MPa) [50]	29 nm	840	↘	335	25 °C	240	↗	840
	9 nm	240	↘	90	100 °C	90	↗	335
K (MPa) [52]	2400		↗	1100	cst			
γ (N/m) [51]	$3.6\ 10^{-2}$		↘	$3.1\ 10^{-2}$	cst			
C [48,49]	0.5		↗	0.8	~cst			
B[a]	cst				~cst			
δ[a]	~cst				cst			

[a] Both B and δ are assumed to be constant.

to cavitation that does not enable an accurate determination of ε_{onset}. The σ^{cav}_{macro} data in the pre-yield strain domain are plotted in Fig. 8 as a function of L_c for various values of the draw temperature. σ^{cav}_{macro} appears to be very little sensitive to L_c at every T_d whereas it strongly decreases with increasing T_d.

A thorough characterization of Eq. (17) requires to identify the $(\delta^{0.5}B)^{-1}$ term by fitting the data of Fig. 8, since both δ and B are unknown. The values of the parameters C and γ are taken from literature [48–51], whereas K is obtained by extrapolation of data from literature [52]. The E and ϕ_c data directly come from the present experiments. The fittings of the experimental data at the various temperatures give a fairly constant value $(\delta^{0.5}B)^{-1} = 0.42 \pm 0.04$. This result is quite remarkable since it validates our assumptions that both δ and B are roughly constant. Indeed, if the constant value of B was justified on scientific grounds it was not the case for δ. Moreover, $(\delta^{0.5}B)^{-1}$ is the only adjustable parameter of the present cavitation model. Its constant value irrespective of temperature and crystal thickness reveals an excellent robustness of the model.

It is to be noticed that the strong temperature dependence of the σ^{cav}_{macro} experimental data does not appear strikingly from Eq. (17). The observed T_d independence of the $(\delta^{0.5}B)^{-1}$ term as well as the rather low T_d sensitivity of γ and K [51,52] suggest that the experimental temperature dependence of σ^{cav}_{macro} mainly lies in the C and E parameters. As a matter of fact, in the temperature range 25–100 °C, C increases from 0.5 to 0.8 whereas E drops by a factor of about 2–3 for any sample (see Table 3). These two factors can mainly account for the σ^{cav}_{macro} drop with increasing T_d (Fig. 8).

Regarding the modeling of the crystalline shear process, the present work borrows from the physically supported dislocation approach proposed by Young [53] which is the most consensual one so far. Indeed, several authors have checked the robustness this approach as a function of experimental parameters such as temperature and strain rate as well as structural parameters such as crystallinity and/or crystal thickness (see Ref. [54] and refs cited therein). In this approach the critical tensile stress, σ_{crit}, for initiation of crystal shear was shown to obey a sigmoidal dependence on L_c of the form

$$\sigma_{crit} \propto \exp(-A(T)/L_c - 1) \tag{18}$$

However, in the range of crystal thickness 5–30 nm that corresponds to medium and high crystallinity PE materials, Eq. (18) follows a fairly linear relationship versus L_c, [53], and experimental data as well at RT. So that Eq. (18) can be approximated by

$$\sigma_{crit} = \alpha(T)\, L_c \tag{19}$$

Moreover, in a previous paper regarding specifically the yielding behavior of the present materials at room temperature, Humbert et al. [44] showed that the linear relationship is strongly sensitive to the crystallization method. This dependence was ascribed to the modification of the molecular topology of the amorphous phase which transmits the stress between the crystal lamellae via tie molecules, chain entanglements, rigid amorphous interfacial layer, etc This contribution was empirically taken into account by the relation

$$\sigma_{yield} \propto \sigma_{crit}[ST]^{0.6} \tag{20}$$

where σ_{yield} is the actual tensile stress for yielding and [ST] is the concentration of molecular stress transmitters in the amorphous phase. In parallel, it was experimentally observed [23] that $[ST] \propto L^{-0.5}$.

Thus, it finally results that σ_{yield} can be expressed as

$$\sigma_{yield} = \alpha(T)\, L_c^{0.7} \tag{21}$$

where α is a function of the temperature.

Experimental σ_{yield} data have been plotted in Fig. 9 as a function of L_c, for the various values of the draw temperature. These data display first a monotonic increase with increasing L_c. The temperature dependence is also fairly monotonic. However, a very clear deviation appears for the higher L_c values when σ_{yield} levels off. This is particularly noticeable for the lower T_d values, i.e. 25 °C and 50 °C, and for the samples which displayed homogeneous cavitation prior to yielding. Besides, the strain level at which the deviation starts coincides with the ε_{onset} for cavitation. This is an indication that the early occurrence of cavitation, i.e. homogeneous cavitation, biases the onset of the yielding process at a stress value lower than it should be if yielding occurred by crystal shear only. It is to be noticed that this phenomenon of cavitation-promoted yielding has been already discussed by some authors without experimental evidence [14,25]. In the present study, the σ_{yield} data in the deviation strain domain of Fig. 9 have been excluded for the fitting of Eq. (21). This fitting was fairly well achieved by the following function

$$\sigma_{yield} = (\alpha T + b)\, L_c^{0.7} \tag{22}$$

where $a = -0.036$ and $b = 14.6$, when σ_{yield} is given in MPa, L_c in nm and T in °C.

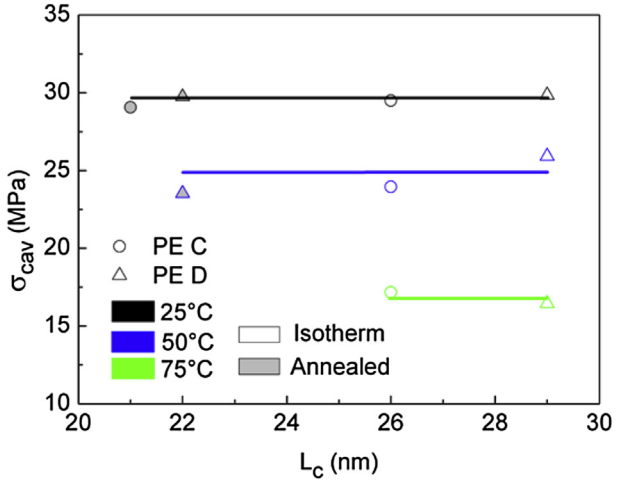

Fig. 8. Experimental σ^{cav}_{macro} data for samples displaying homogeneous cavitation as a function of L_c and for various T_d values.

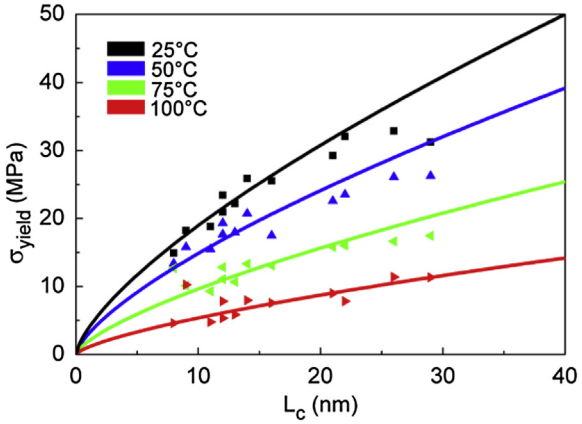

Fig. 9. Experimental σ_{yield} data as a function of L_c.

In the purpose of predicting the cavitation/shear competition, Eq. (17) and Eq. (21) have been plotted together in Fig. 10 as a function of L_c, for the various draw temperatures investigated in the present study. It clearly appears that σ_{cav} is considerably less sensitive to L_c than σ_{yield}. However, the dependence on temperature is quite similar for the two processes: as a matter of fact, it can be seen that over the whole L_c range of Fig. 10 the value of either σ_{cav} or σ_{yield} at 75 °C is close to half the corresponding value at 25 °C.

It is to be noticed that the present theoretical modeling of cavitation predicts a rather low dependence of σ^{cav}_{macro} on L_c in contrast to the previous qualitative approach predicting a noticeable drop of the cavitation stress increasing L_c. The reason is that the meso-macro scale transition was not taken into account in the previous study.

The macroscopic stress for cavitation was supposed identical to the stress at the meso scale σ^a_z (Fig. 7). This stress has been shown to strongly depend on the stress concentration of transmitters, [ST], that decreases with increasing crystal thickness. More details on this σ^a_z dependence on [ST] and L_c are given in appendix. However, the meso-macro scale transition introduced in the present work involves a compensation effect leading to a predicted weak dependence of σ^{cav}_{macro} on L_c.

Comparing now the evolutions of σ^{cav}_{macro} and σ_{yield} at every temperature, the major feature of Fig. 10 is that every couple of curves exhibits a crossing point at a critical L_c value, L_{cc}, to which is associated a change in the deformation regime. The occurrence of this crossing point is due to the strong dependence of σ_{yield} on L_c whereas σ^{cav}_{macro} is essentially L_c independent. For $L_c < L_{cc}$, σ_{yield} is lower than σ^{cav}_{macro} so that crystal shear is expected to start before the occurrence of cavitation; for $L_c > L_{cc}$, σ_{yield} is higher than σ^{cav}_{macro} so that cavitation is expected to start before the occurrence of crystal shear followed by yielding. It is to be noticed that Fig. 10 only applies for homogenous cavitation, it does not predict the occurrence of heterogeneous cavitation.

The L_{cc} data predicted from Fig. 10 are plotted in Fig. 11 as a function of the draw temperature, only for the material which displayed homogeneous cavitation, i.e. the annealed and isotherm samples of polymers PE-C and PE-D. The steady increase of L_{cc} with temperature is an indication that the occurrence of crystal shear prior to cavitation in the case of thick crystalline lamellae requires an increase of the draw temperature. For the sake of comparison, experimentally determined values of L_{cc} are also plotted in Fig. 11. These experimental L_{cc} values were computed at every T_d from the average of the higher L_c value for which crystal shear initiates first

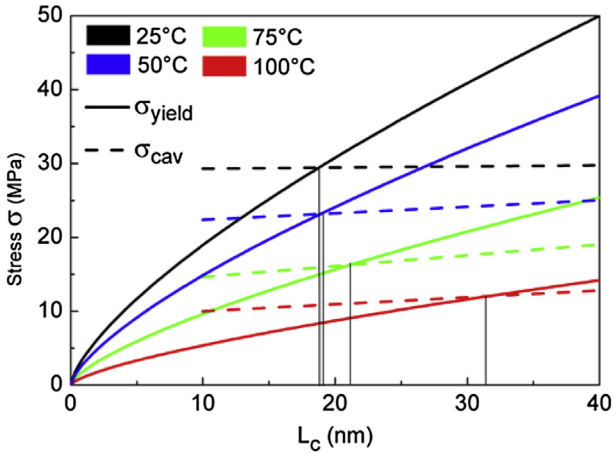

Fig. 10. Predicted evolution of σ_{cav} and σ_{yield} as function of L_c for various values of the draw temperature.

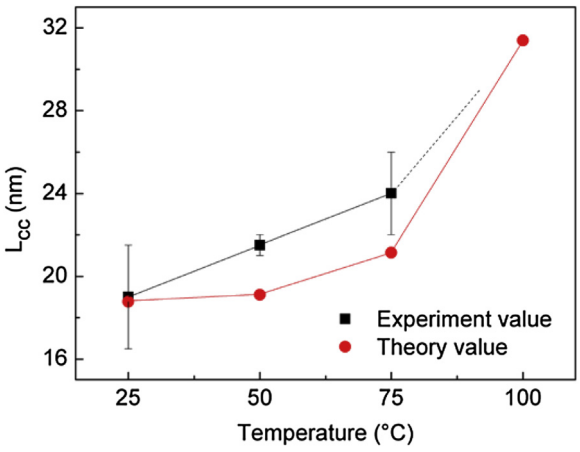

Fig. 11. Predicted and experimental L_{cc} values as a function of draw temperature for the annealed and isotherm samples of polymers PE-C and PE-D.

and the lower L_c value for which cavitation occurs first. For example, at $T_d = 25$ °C, crystal shear is activated first for $L_c \leq 16$ nm whereas cavitation occurs first for $L_c \geq 21$ nm: then $L_{cc} = 19 \pm 3$ nm.

Because none of the present samples exhibit initiation of cavitation before crystalline shear at 100 °C, it can be concluded that at this temperature L_{cc} is above the higher L_c value of the present study, i.e. 29 nm for PE-D isotherm. This perfectly agrees with the predicted value $L_{cc} = 32$ nm at $T_d = 100$ °C (Fig. 11).

5. Conclusion

The aim of the present study was to address the phenomenon of cavitation in semi-crystalline polymers on both experimental and theoretical standpoints. Either homogeneous or localized cavitation has been observed before or after yielding. A comparison between the strain onset of cavitation and the yield strain clearly showed the competition between the two phenomena. The crystal thickness proved to be a major structural factor of the competition together with the temperature. Moreover, it was clearly shown that the occurrence of homogeneous cavitation prior to yielding promotes the occurrence of crystal shear as evidenced by the yield stress depression.

In the temperature range 25–100 °C, homogeneous cavitation prior to yielding was observed only for samples having $L_c > 20$ nm. Localized cavitation after yielding occurred for samples having $L_c > 12$ nm, depending on the draw temperature, T_d. In contrast, no cavitation was observed for samples having $L_c < 12$ nm, the plastic deformation being fairly homogeneous. For samples of this kind, homogenous cavitation would eventually occur below RT. The main influence of an increase of T_d was to either promote localized cavitation after yielding for samples that displayed homogeneous cavitation at RT, or to inhibit cavitation in the case of localized cavitation at RT.

Regarding the modeling of strain-induced cavitation, a thermally activated nucleation of voids in the amorphous layers of the lamella stacks has been developed for the equatorial regions of the spherulites where the local stress is normal to the lamella surface. A 2-step scaling transition from the micro- to the macro-scale can be easily achieved via the meso-scale of the stacks. It is worth noticing that this modeling involves only one adjustable parameter $(\delta^{0.5}B)^{-1}$ where the microstructural parameter B is hardly accessible to experiments and δ is generally used to account for complex phenomena not taken into account in the classical nucleation theory. The very low sensitivity of σ^{cav}_{macro} to crystal thickness and its strong dependence on T_d are fairly well predicted.

Two remarks have to be made regarding the shortcomings of the cavitation modeling and the limits of the approach for predicting the cavitation/yielding competition. First, the cavitation nucleation model only applies to semi-crystalline polymers having a high shape factor of the crystalline lamellae, i.e. relatively high crystallinity polymers ($X_c \geq 50\%$). Indeed, for low crystallinity materials the B coefficient could not be considered as independent of the shape factor (see comment of Eq. (9)). For this reason the domain $L_c < 10$ nm that corresponds to low crystallinity materials should be excluded from the modeling, though the prediction of no cavitation in Fig. 10 does reflect the actual observations. Second, the present modeling of the yielding process does not apply to very thick crystals (i.e. $L_c \geq 40$ nm) for which it turns out that the yield stress levels off [55]. Fortunately, a good deal of polyethylene materials fall in the domain 10 nm $< L_c <$ 40 nm.

In parallel to the cavitation modeling, a semi-empirical approach has been proposed to describe for the dependency on temperature and crystal thickness of the yield stress, borrowing from previous theoretical and experimental studies.

The comparison of the predicted σ^{cav}_{macro} and σ_{yield} curves allows determining the L_c domains where either of the two processes occurs first. For every T_d value, a shear/cavitation transition clearly appears for a critical value of the crystal thickness, L_{cc}. The main influence of increasing T_d was to shift L_{cc} to higher values. This was not intuitively predictable since the two challenging processes display similar T_d dependence at first sight (Fig. 10). The fact is that the T_d dependence of σ_{yield} is slightly stronger than that of σ^{cav}_{macro} which is not totally explicit in Eq. (17) due to the temperature dependence of several material parameters. Therefore, owing to its greater temperature sensitivity yielding becomes predominant over cavitation with increasing T_d: it results that samples having increasingly thick crystals may yield without cavitation at high T_d.

The predicted L_{cc} values thus determined from the crossing of the modeled curves are remarkably close to the ones experimentally observed, at every draw temperature.

To finish with, it must be pointed out that our modeling approach should a priori apply to most kinds of semi-crystalline polymers provided that the crystal shear stress obeys a growing monotonic relationship with L_c, in agreement with Young's dislocation-governed model.

Acknowledgments

The European Synchrotron Radiation Facility (ESRF, Grenoble, France) is gratefully acknowledged for time allocation on the BM02/D2AM line. The authors are indebted to the China Scholarship Council for the grant of a doctoral fellowship to B. Xiong.

Appendix. Role of [ST] on σ_{cav}

Equation (A) is related to the stress state in the lamellar stack (see Eq. (9) in the text). It is supposed to be dependent on the geometry of the stack. For a very high shape factor (f = length/thickness) the behavior is nearly oedometric: the lateral contraction when stretching normal to the lamella surface is negligible. In this case $B = 1$. When the shape factor is very low, i.e. $f \approx 1$, stretching normal to the lamella surface can be assimilated to a simple tensile test: then $B = 0$, i.e. isovolumic deformation for a rubber.

$$\varepsilon_v = B\varepsilon_z^a \quad (A)$$

It is now possible to rewrite this equation by introducing the stress, assuming linear elastic behavior,

$$\sigma_v = K\varepsilon_v \quad (B)$$

$$\sigma_z^a = M\varepsilon_z^a \quad (C)$$

where M is the apparent modulus of the confined amorphous phase. By combining Eqs. A–C, a stress relation can be obtained:

$$\sigma_z^a = \frac{M}{KB}\sigma_v \quad (D)$$

The micro-macro relationship between the macroscopic stress and the axial stress in the stack into the following form can then be rewritten:

$$\sigma_{macro} = \sigma_z^a \frac{E_{macro}}{C\,M}(1 - \Phi_c) \quad (E)$$

Regarding the dependence of σ_z^a with L_c, one can notice that C and $E(1-\phi_c)$ are roughly independent of L_c. As a consequence, considering only the L_c variation, it turns out that

$$\sigma_{macro} \propto \frac{\sigma_z^a}{M} \quad (F)$$

As σ_{macro} is only weakly dependent with L_c, there are two possibilities. Either both σ_z^a and M are independent of L_c or they evolve in opposite sense. However there are strong clues [56] that ST reinforce the amorphous phase a then that M is a growing function of the concentration of stress transmitters [ST]. Moreover, it has been shown that [ST] $\propto L_c^{-0.5}$. As a consequence M is likely a decreasing function of L_c. Therefore σ_z^a is decreasing function of L_c as assumed by Humbert et al. [23]: it was indeed assumed that the mesoscale cavitation stress was a growing function of [ST].

References

[1] Friedrich K. Adv Polym Sci 1983;52/53:225–73.
[2] Narisawa I, Ishikawa M. Adv Polym Sci 1990;91/92:353–91.
[3] Plummer CJG. Adv Polym Sci 2004;169:75–119.
[4] Galeski A. Prog Polym Sci 2003;28:1643–99.
[5] Plummer CGJ, Kausch H-H. Macromol Chem Phys 1995;197:2047–63.
[6] Butler MF, Donald AM, Bras W, Mant GR, Derbyshire GE, Ryan AJ. Macromolecules 1995;28:6383–93.
[7] Butler MF, Donald AM, Ryan AJ. Polymer 1997;38:5521–38.
[8] Butler MF, Donald AM, Ryan AJ. Polymer 1998;39:39–52.
[9] Butler MF, Donald A. Macromolecules 1998;31:6234–49.
[10] Castagnet S, Girault S, Gacougnolle JL, Dang P. Polymer 2000;41:7523–30.
[11] Michler GH, Godehardt R. Cryst Tes Technol 2000;35:863–75.
[12] Men YF, Rieger J, Homeyer J. Macromolecules 2004;37:9481–8.
[13] Schneider K, Trabelsi S, Zafeiropoulos NE, Davies R, Riekel C, Stamm M. Macromol Symp 2006;236:241–8.
[14] Pawlak A, Galeski A. Macromolecules 2005;38:9688–97.
[15] Pawlak A. Polymer 2007;48:1397–409.
[16] Pawlak A, Galeski A. Macromolecules 2008;41:2839–51.
[17] Pawlak A, Galeski A. J Polym Sci Polym Phys 2010;48:1271–80.
[18] Pawlak A, Galeski A. Polymer 2010;51:5771–9.
[19] Rozanski A, Galeski A, Debowska M. Macromolecules 2011;44:20–8.
[20] Na B, Lv R. J Appl Polym Sci 2007;105:3274–9.
[21] Thomas C, Ferreiro V, Coulon G, Seguela R. Polymer 2007;48:6041–8.
[22] Baravian C, Andre S, Renault N, Moumini N, Cunat C. Rheol Acta 2008;47:555–64.
[23] Humbert S, Lame O, Chenal JM, Rochas C, Vigier G. Macromolecules 2010;43:7212–21.
[24] Fischer S, Diesner T, Rieger B, Marti O. J Appl Crystallogr 2010;43:603–10.
[25] Zhang X, Schneider K, Liu G, Chen J, Brüning K, Wang D, et al. Polymer 2012;53:648–56.
[26] Patlazhan S, Remond Y. J Mater Sci 2012;47:6749–67.
[27] Kramer EJ. Adv Polym Sci 1983;52–53:1–56.
[28] Bowden PB, Young RJ. J Mater Sci 1974;9:2034–51.
[29] Lin L, Argon AS. J Mater Sci 1994;29:294–323.
[30] Liu TM, Juska TD, Harrison IR. Polymer 1986;27:247–9.
[31] Men Y, Rieger J, Strobl G. Phys Rev Lett 2003;91(095502):1–4.
[32] François P, Gaucher V, Seguela R. J Phys Cond Matter 1994;6:8959–68.
[33] Castagnet S, Gacougnolle J-L, Dang P. J Mater Sci 1999;34:5133–8.
[34] Gloaguen J-M, Lefebvre J-M. Polymer 2001;42:5841–7.
[35] G'Sell C, Hiver J-M, Dahoun A. Intern J Solids Struct 2002;39:3857–72.
[36] Castagnet S, Tence-Girault S. J Macromol Sci Phys 2002;B41:957–76.
[37] Addiego F, Dahoun A, G'Sell C, Hiver J-M. Polymer 2006;47:4387–99.
[38] Castagnet S, Girard D. J Mater Sci 2007;42:7850–60.
[39] Addiego F, Dahoun A, G'Sell C, Hiver J-M. Polym Eng Sci 2009;49:1198–205.

[40] Wunderlich B. Macromolecular physicsIn Crystal structure, morphology, defects, vol. 1. New York: Academic Press; 1973.
[41] http://www.esrf.eu/UsersAndScience/Experiments/CRG/BM02/detectors/ccd.
[42] Humbert S. INSA de Lyon (France). PhD Thesis; 2009.
[43] Stribeck N. X-ray scattering of soft matter. Berlin Heidelberg: Springer-Verlag; 2007.
[44] Humbert S, Lame O, Vigier G. Polymer 2009;50:3755–61.
[45] PhD Thesis Mourglia-Seignobos E. INSA de Lyon (France); 2009.
[46] Kashchiev D. Nucleation: basic theory with applications. Oxford UK: Butterworth; 2000.
[47] Fond C. J Polym Sci Polym Phys 2001;39:2081–96.
[48] Humbert S, Lame O, Chenal JM, Rochas C, Vigier G. J Polym Sci Polym Phys 2010;48:1535–42.
[49] Xiong B, Lame O, Chenal JM, Vigier G. To be published.
[50] Humbert S, Lame O, Seguela R, Vigier G. Polymer 2011;52:4899–909.
[51] Wu SJ. Colloid Interface Sci 1969;31:153–61.
[52] Crine JP. Polym Bull 1986;15:375–80.
[53] Young RJ. Philos Mag 1974;30:85–94.
[54] Seguela R. J Polym Sci Polym Phys 2002;40:593–601.
[55] Kazmierczak T, Galeski A, Argon AS. Polymer 2005;46:8926–36.
[56] Makke A, Lame O, Perez M, Barrat JL. Macromolecules 2012;45:8445–52.

Glossary

X_c: crystal weight-fraction.
ϕ_c: crystal volume-fraction.
T_d: draw temperature.
L_p, L_c, L_a: long period of the lamella stacks, crystal thickness, amorphous layer thickness.
V: volume fraction of voids as measured by SAXS.
ε: macroscopic strain.
ε_{onset}: strain onset of cavitation determined by SAXS.
K: bulk modulus of the rubbery material.
γ: surface tension of the cavity in the rubbery amorphous phase.
r: radius of cavity.
r_c: critical radius for nucleation of a cavity.
φ: potential energy of the rubbery material undergoing cavitation.
$\Delta\varphi$: potential energy barrier for cavitation of the form $\Delta\varphi = \delta k_b T$.
k_b: Boltzmann constant
ε_v^{cav}: volume strain generated by a cavity in the homogeneous rubbery material.
σ_v^{cav}: volume stress or hydrostatic stress for the nucleation of a cavity.
ε_z^a: mesoscopic axial strain in the amorphous phase in the lamella stacks.
σ_z^a: mesoscopic axial stress in the amorphous phase (σ_z^a refers to σ_{cav} from ref.23)
B: proportionality coefficient between ε_v and ε_z^a.
f: shape factor length/width of the crystalline lamellae.
ε_v: mesoscopic volume strain in the amorphous phase in the lamella stacks.
σ_v: volume stress in the amorphous phase in the lamella stacks.
ε_{meso}: axial strain at the mesoscale of the lamella stack as measured by SAXS.
ε_{macro}: macroscopic axial strain.
C: proportionality coefficient between ε_{meso} and ε_{macro}.
E: Young modulus of the bulk material.
σ_{macro}: macroscopic tensile stress
σ_{macr}^{ocav}: macroscopic tensile stress for initiation of cavitation.
ε_{yield}: strain at yield point.
σ_{crit}: critical tensile stress for initiation of crystal shear from Young's dislocation model.
σ_{yield}: actual tensile stress for yielding.
[ST]: concentration of molecular stress transmitters between crystalline lamellae.
L_c^{min}: minimum value of crystal thickness for which cavitation can occur at given T_d.
L_{cc}: critical crystal thickness at the crystal shear / cavitation transition.
M: apparent elastic modulus of the amorphous phase.